CFD Analysis of Laminar Natural Convection from a Horizontal Circular Cylinder to its Concentric Elliptic Enclosure

Hojjat Khozeymeh Nezhad
PHD student, Mechanical Engineering, Ferdowsi University of Mashhad
Khozeymeh.hojat@gmail.com

Hamid Niazmand
Professor, Department of Mechanical Engineering,Ferdowsi University of Mashhad
niazmand@um.ac.ir

Seyyed Ali Mirbozorgi
Assistant Professor, University of Birjand
samirbozorgi@birjand.ac.ir

Abstract

In the present paper, using a two-dimensional numerical simulation, the heat transfer from a hot circular cylinder to a cold vertical elliptic enclosure has been studied parametrically. The effect of ratio of cylinder radius to the half minor axis length of vertical elliptic enclosure (R/b) *on the rate of the heat transfer has been investigated for the Rayleigh number* 10^4 *and* 10^5*. Governing equations have been solved using the finite volume method and TDMA in an ADI procedure. Results show that the patterns of streamlines, isotherms and the Nusselt number values depend strongly on Rayleigh number and ratio of* R/b*. Furthermore, it is observed that by increasing the Rayleigh number and the ratio of* R/b*, the heat transfer rate is increased. For instance, when the* R/b *value is changed from 0.2 to 0.6 at* $Ra = 10^5$*, the Nusselt number is increased about 55 percent of its initial value. Also when the Raleigh number is risen from* 10^4 *to* 10^5 *at* $R/b = 0.6$*, the Nusselt number is climbed almost 65 percent of its initial value.*

Key words: CFD Analysis, Natural Convection, Hot Circular Cylinder, Cold Elliptic Enclosure, Vortex, Finite Volume Method.

1. Introduction

So far, many studies in the field of natural convection inside simple enclosures have been performed so that it is a classic problem now. However, the natural convection heat transfer problem inside enclosures with non-simple shape and in the presence of internal bodies with different geometry is a topic that has been recently received more attentions. Based on the published papers in this field, it can be claimed that the subject has been seriously investigated with the development of numerical methods and related hardwares in the past two decades. The present problem has many applications such as convection in buildings, fluid movement in solar energy collectors, cooling of electronic circuits, cooling of nuclear reactors, aircraft cabin insulation, transmission cable cooling systems, and food processing, etc.

Various aspects of this topic have been studied numerically and experimentally yet. For example, the shape of enclosure can have different forms including square, triangle, and

circle, etc. In this regard, Xu et al. [1] , Sheikholeslami et al. [2], Roslan et al. [3] and da Silva et al. [4] chose triangle, circle, square and trapezoid enclosure respectively for studying of natural convection.

The other aspect related to the subject about which there are many studies is different numerical methods using to solve the governing equations of natural convection flow inside enclosures so that they lend themselves to the application of different numerical techniques. For instance, Mark et al. [5], Oztop et al. [6], Mahmoodi and Sebdani [7] and Mouhtadi et al. [8] using the immersed boundary method, Galerkin weighted residual finite element method, finite volume method and finite difference method to solved the governing equations of natural convection inside a square enclosure respectively.

The other interesting aspect about which there are many studies but still it requires more researches is shape and size of the internal body, its location and various boundary conditions. In the following, some papers in this field are reviewed in details. Mota et. al. [9] carried out a numerical investigation of natural convection in horizontal eccentric elliptic annuli containing saturated porous media. Governing equations were solved in a generalized orthogonal coordinate system, using high-order compact finite difference. In addition, the mesh was generated numerically using the orthogonal trajectory method. Effects of geometric parameters such as eccentricity, ratios of axes length of elliptic enclosure as well as cylinder is investigated on heat transfer rate at the constant $Ra = 100$ and hydraulic-radius ratio(=2). Results showed that the heat losses could be minimized by a proper choice of the elliptic shape of a concentric annulus, which can be further enhanced if the geometry is made eccentric.

Zhu et. al. [10] considered a hot elliptic cylinder inside a cold elliptic enclosure and performed a numerical simulation of natural convection inside the enclosure using the differential quadrature (QD) method. The governing equations were solved for the analysis of flow and thermal fields at different eccentricities and angular positions at only $Ra = 10^4$. Results showed that the position of the major axis of the inner elliptic cylinder has an important effect on the streamlines, and very few effects on the average Nusselt number. In addition, when the major axis of the cylinder is in a vertical position, the maximum stream function value is increased, and in general, the average Nusselt number is slightly higher than that in a horizontal position.

J. Habeeb [11] carried out a numerical study of laminar natural convection around a hot square cylinder inside a cold elliptic enclosure. The finite difference method is used to solve the governing equations. The effects of different ratios of the geometry such as, ratio half major axis length to half minor axis length of elliptic enclosure (a/b) and ratio characteristic length of square cylinder to half minor axis length of elliptic enclosure (l/b) and the Rayleigh number from 10^3 to 10^6, for two position of the major axis of the elliptic enclosure, horizontal and vertical. Results show that, by increasing the a/b ratio, the average Nusselt number is also increased and the flow strength is decreased for all Rayleigh numbers.

Khozeymehnezhad and Mirbozorgi [12] carried out a numerical solution for comparison of the natural convection around a circular cylinder with a square cylinder inside a square enclosure. They studied the effects of cross section of cylinder as well as its vertical location change on heat transfer rate from enclosure. Results showed that the heat transfer rate from the enclosure with circular internal cylinder is better than other internal cylinder in all studied cases.

The above relevant literature survey shows that even though the fundamental features of natural convection inside enclosures have been identified and analyzed, in most cases, the effects of natural convection around inner circular cylinders inside an elliptic enclosure have not examined in detail. Of particular interest is the study of effect of ratio of cylinder radius to half minor axis length of elliptic enclosure (R/b) on the rate of the heat transfer. However, few studies were performed on investigation of the effect of high R/b value on heat transfer rate of enclosure. It can be claimed that no work in which the effect of R/b higher than 0.8 was studied on heat transfer rate, was observed by the authors. In this regard, in the present study, different features of the natural convection around the circular cylinder inside an elliptic enclosure are investigated numerically for various Rayleigh numbers and different ratios of R/b.

2. Physical Model and Assumptions

Fig. 1 shows a schematic of the system considered in the present study which consists of a vertical elliptic enclosure with half major axis length of *a* as its characteristic length and half minor axis length of *b* (here: $a = 1.5b$). In addition, a circular cylinder with the radius of *R* is located in the center of this enclosure. Here, the ratio of R/b can change in the range of 0.01 to 0.95.

The wall of the elliptic enclosure was kept at a constant low temperature of T_c whereas the internal cylinder was kept at a constant high temperature of T_h. The fluid properties are also assumed to be constant, except for the density in the buoyancy term, that follows the Boussinesq approximation in which the fluid density is considered as $\rho = \bar{\rho}\big(1 - \beta(T - T_c)\big)$ where $\bar{\rho}$ is the average density. All of the calculations are performed at two values of Rayleigh numbers namely $Ra = 10^4\ and\ 10^5$. Prandtl number, Pr, is 0.71 corresponding to that of air.

3. Governing Equations

In order to state the governing equations in a dimensionless form, the following dimensionless variables are defined:

$$X = \frac{x}{H}, Y = \frac{y}{H}, U = \frac{uH}{\alpha}, V = \frac{vH}{\alpha}, P = \frac{pH^2}{\rho\alpha^2}, \theta = \frac{T - T_c}{T_h - T_c} \tag{1}$$

Based on the above dimensionless variables, the non-dimensional form of the equations for the conservation of mass, momentum and energy are:

$$\frac{\partial \mathrm{U}}{\partial \mathrm{X}} + \frac{\partial \mathrm{V}}{\partial \mathrm{Y}} = 0 \tag{2}$$

$$\mathrm{U}\frac{\partial \mathrm{U}}{\partial \mathrm{X}} + \mathrm{V}\frac{\partial \mathrm{U}}{\partial \mathrm{Y}} = -\frac{\partial \mathrm{P}}{\partial \mathrm{X}} + \mathrm{Pr}\left(\frac{\partial^2 \mathrm{U}}{\partial \mathrm{X}^2} + \frac{\partial^2 \mathrm{U}}{\partial \mathrm{Y}^2}\right) \tag{3}$$

$$\mathrm{U}\frac{\partial \mathrm{V}}{\partial \mathrm{X}} + \mathrm{V}\frac{\partial \mathrm{V}}{\partial \mathrm{Y}} = -\frac{\partial \mathrm{P}}{\partial \mathrm{Y}} + \mathrm{Pr}\left(\frac{\partial^2 \mathrm{V}}{\partial \mathrm{X}^2} + \frac{\partial^2 \mathrm{V}}{\partial \mathrm{Y}^2}\right) + RaPr\theta \tag{4}$$

$$\mathrm{U}\frac{\partial \theta}{\partial \mathrm{X}} + \mathrm{V}\frac{\partial \theta}{\partial \mathrm{Y}} = \frac{\partial^2 \theta}{\partial \mathrm{X}^2} + \frac{\partial^2 \theta}{\partial \mathrm{Y}^2} \tag{5}$$

Where the Rayleigh, *Ra* and Prandtl, *Pr* numbers are defined:

$$Ra = \frac{g\beta(T_h - T_c)H^3}{\propto\vartheta}, \Pr = \frac{\vartheta}{\alpha} \quad (6)$$

The dimensionless boundary conditions are:

On the walls of enclosure: U = V = 0 ; θ= 0 (7)

On the heated cylinders: U = V = 0 ; θ = 1 (8)

In the analysis, the average Nusselt number is defined as:

$$Nu = \left.\frac{\partial\theta}{\partial n}\right|_{\text{wall}}, \quad \overline{Nu} = \frac{1}{S}\int_0^S \text{Nu } dS \quad (9)$$

Where n is the normal direction with respect to the walls and S is distance along the square enclosure

4. Numerical Method

4.1. Numerical procedure

Fig. 2 shows algebraic generated grid around a circular cylinder with $R/b = 0.95$ inside a vertical elliptic enclosure. This non-orthogonal grid has been applied for solution of the non-dimensional equations subject to their boundary conditions. Near the walls of enclosure and inner cylinder where the temperature distribution takes a high gradient, a high grid concentration is required to resolve the temperature distribution accurately. In this regard, as it can be seen in the figure 2, expansion factors near the circular cylinder and the elliptic enclosure walls are adopted $f_1 = 1.04$ and $f_2 = 1.04$ respectively.

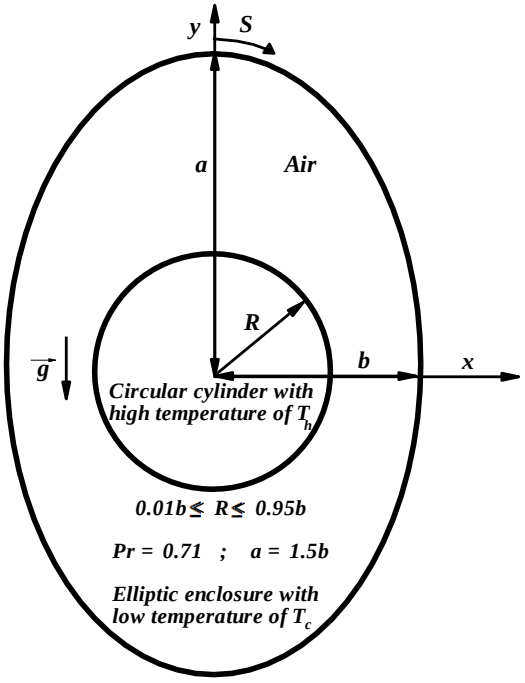

Fig. 1: Schematic of system along with boundary conditions

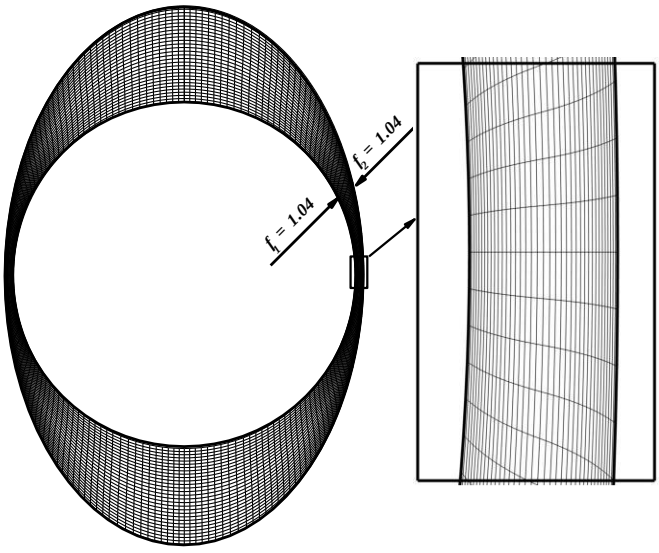

Fig. 2: An algebraic generated grid around a circular cylinder with $R/b = 0.95$ inside an elliptic enclosure.

The set of coupled governing Eqs. (2)-(5) is discretized using finite volume method. In this method, equations are integrated over an arbitrary control volume to obtain a set of discretized linear algebraic equations in the form of the:

$$a_P \emptyset_P = \sum a_{Nb} \emptyset_{Nb} + S \tag{10}$$

The *SIMPLE* [13] algorithm handles the linkage between velocity and pressure fields. However, to avoid the likely checkerboard effect in the pressure field due to the use of collocated variables, the interpolation scheme of Rhie-Chow [14] is used to calculate the convecting mass flow rates. The diffusion terms in the equations are discretized by a second order central difference scheme, while a hybrid scheme is employed to approximate the advection and diffiusion terms simultaneously. The resulting algebraic system of equations is then solved using an *ADI* iterative method with the tri-diagonal matrix algorithm (*TDMA*) [15].

In this algorithm, first, the computations of flow field begin with a guessed pressure field, and the momentum equations are solved to obtain the velocity field. Using this velocity field, the continuity equation is solved to correct the pressure and velocity fields as described by Van Doormaal and Raithby [13]. Then the temperature is obtained by solving the energy equation. This iterative solution continues to reach convergence criteria according to the following definitions:

$$R_P = a_P \emptyset_P - \left(\sum a_{Nb} \emptyset_{Nb} + S \right) \tag{11}$$

The convergence criterion for each equation can be defined as follows:

$$Res = \sum_P |R_P| \tag{12}$$

Where p is central point in each aforementioned arbitrary control volume.

To normalize the residual (Res) of each equation, it is dividing into a reference residual (Res_{ref}), therefore the iterative solution will stop when $\overline{Res} = \frac{Res}{Res_{ref}} < \varepsilon$, where ε is a maximum error of a single precision calculation on a computing machine with the finite representation of number of eight digits namely 10^{-8}.

It should be noted that the reference residual is $\rho A u_{ref}^2$ for momentum equations, $\rho A u_{ref}$ for pressure equation and $\rho C_p A u_{ref} T$ for energy equation. A is the area of ellipse and u_{ref} is a reference velocity that in this paper, it has the maximum value of convective velocity near a vertical wall. Under-relaxation coefficients are $\alpha_u = \alpha_v = 0.45$ for velocity equation, $\alpha_p = 0.35$ for pressure equation and $\alpha_T = 0.55$ for temperature equation.

4.2. Grid Independence Study

To perform the grid independence study, a case of hot circular cylinder with $R/b = 0.4$ inside a cold elliptic enclosure is considered at $Ra = 10^6$. Four different grids, namely, 3500, 11500, 23500 and 30500 are employed for the numerical calculations. The obtained surface-averaged Nusselt number of elliptic enclosure ($\overline{Nu}_{en}$) by each kind of grids is shown in Table 1. In this Table, the ratio of ($\Delta\overline{Nu}_{en}/\overline{Nu}_{en}$) shown in third row is nominated Difference. As it can be seen, the 23500 grids are sufficiently fine for the numerical calculation.

Table 1: The ($\overline{Nu}_{en}$) for different grids

Grids	3500	11500	23500	30500
$\overline{Nu}_{en}$	4.868	4.673	4.586	4.583
Difference (%)	-	4.01	1.86	0.06

4.3. Code validation

To validate the present numerical algorithm a natural convection problem with a low temperature outer square enclosure and a high temperature inner circular cylinder was simulated. The calculated averaged Nusselt numbers for the case at hand are compared with the benchmark values of Kim et al. [16] as shown in Table 2. In this comparison dimensionless parameters, Pr=0.7, $Ra = 10^4 - 10^6$ and δ=0 were identical. A good agreement is observed between the results.

Table 2: Comparison between the averaged Nusselt numbers obtained by the presente work with the results of Kim et al.[16]

Rayleigh number	Nu_{ave}		Deviation (%)
	Kim et al. [16]	Present Study	
10^4	3.414	3.389	0.732
10^5	5.138	5.149	-0.214
10^6	9.390	9.351	0.415

5. Results and Discussion

5.1. Temperature and flow fields as a function of R/b

5.1.1. $Ra = 10^4$

The Figs. 3 and 4 show isotherm and streamline patterns around the circular cylinder with different values of R/b inside the vertical elliptic enclosure at Raleigh number 10^4 respectively. As shown in the Fig. 3, in all ratios (espesialy in low values) of R/b, the isotherms take distance from the top surface of inner cylinder. But it can be discerned that in high value of R/b, a relative symmetric exist. In addition, it can be observed that the accumulation of isotherms around the lower surface of the cylinder is more than that around its top surface particularly in low R/bs. The reason of this subject can be justified as follows: increasing the Ra number, the convection mechanism becomes also important. By climbing the ratio of R/b and decreasing the interior space of enclosure, this relatively significant mechanism is reduced to the prior mechanism i.e. conduction.

As it can be observed in the Fig. 4, in general, due to temperature difference between inner cylinder and the enclosure, the heated fluid goes upward until it encounters the cold top part of enclosure. Then the fluid becomes gradually colder while it moves downward. Consequently, two large vortices form in left and right sides of cylinder. Corresponding to the Fig. 4 (a-b), each mentioned large vortex has only one center in upper half of enclosure while increasing the value of R/b up to 0.4 (Fig. 4 (c)), in addition to mentioned vortex center, one other vortex center appears in lower half of enclosure in each large vortex. The fluid in the bottom part of enclosure must pass through the confined space between the cylinder and enclosure for going to the top part of ellipse. But some streamlines are not able to overcome the friction in this area and they are forced to returne downward. So two smaller inner

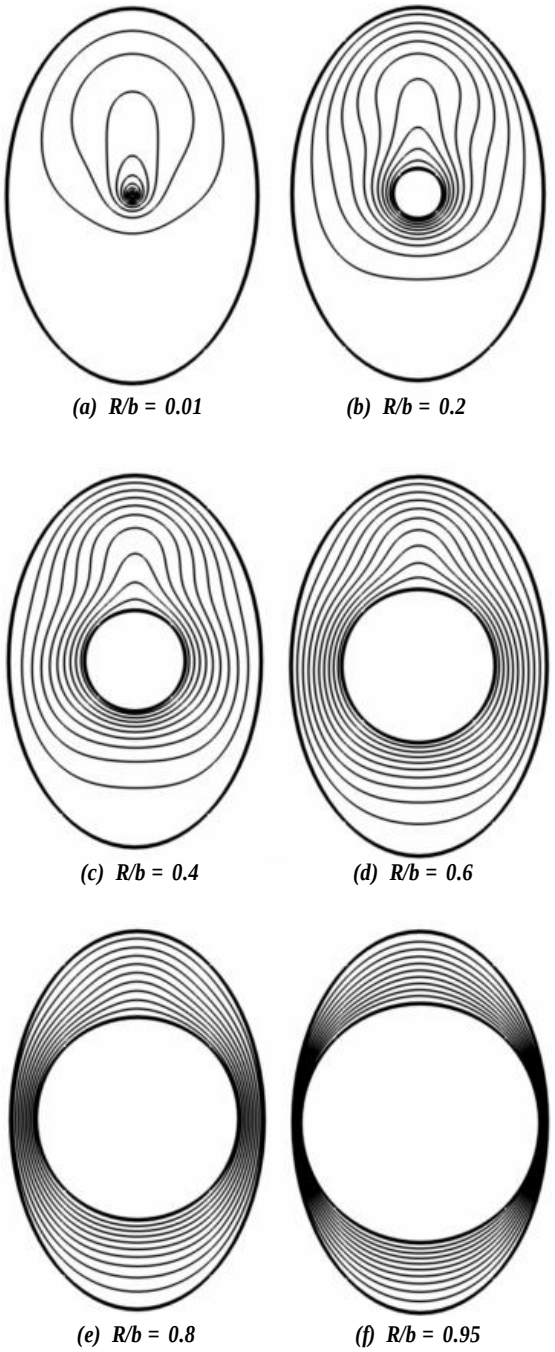

Fig. 3. The isotherms around the hot cylinder inside a cold elliptic enclosure at $Ra = 10^4$

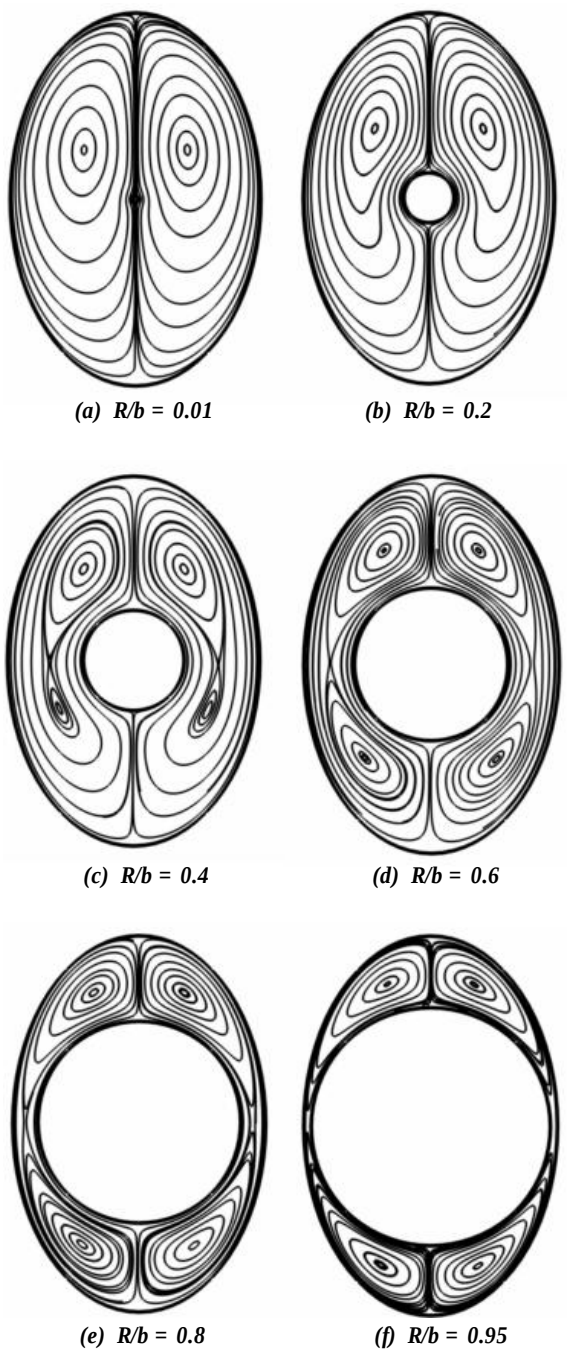

Fig. 4. The streamlines around the hot cylinder inside a cold elliptic enclosure at $Ra = 10^4$

vortices are created in the bottom half of enclosure. Increasing the R/b, corresponding to Fig. 4 (d-f), the same previous trend is repeated and noticeable difference is not perceived between these patterns. At the end, it should be noted that a side effect of two large vortices in the left and right half of enclosure is an upwelling plume that causes to take distance the isotherms from the upper surface of cylinder and accumulate under the top wall of enclosure corresponding to figure 3.

5.1.2. $Ra = 10^5$

The Figs. 5 and 6 show isothems and streamline patterns around the cylinders at $Ra = 10^5$ respectively. According to the Fig. 5, a more intensive rising of isotherms from the upper surface of cylinder and more accumulation of them are observed in the vicinity of the lower part of cylinder as well as the upper wall of enclosure. This is due to increasing the Raleigh number and convective flow effect inside the enclosure. Contrary to the Fig. 3, for $Ra = 10^4$, it is observed that here for $Ra = 10^5$, the isotherms have taken an obvious kink at the upper half of the enclosure. This due to the effect of enforced convection flow near the hot cylinder as the main source of fluid motion.

As it is mentioned that the Fig. 6 shows the streamlines inside the enclosure at $Ra = 10^5$. In general, these patterns are similar to those in the Fig. 4. But there are several differences between them that are mentioned in below.

As it can be observed in the Fig.6 the centers of vortices in the upper half of enclosure shift toward top wall of enclosure as well as the centers of vortices in the lower half of enclosure are drawn upward corrosponding to the Fig. 6 (d-f). The bifurcation from the inner uni-cellular vortex to the bi-cellular vortices occurs at $R/b = 0.6$, which is later than that for the previous case at the $Ra = 10^4$ which appeares at $R/b = 0.4$. This is due to increase of convective flow, by increasing the Ra number. At the end, it should be mentioned that owing to intensifying of convective flow inside the enclosure and subsequently invigoration of plume above the cylinder, the isotherms take more distance from the surface of cylinder than those in the Fig. 3.

5.2. Local Nusselt number

First, it should be mentioned that the Nusselt distribution will be explained in only one half of enclosure namely its right half due to a symmetry with respect to the vertical centerline through the center of the inner cylinder. The Fig. 7 displays the local Nusselt distribution along the wall of the elliptic enclosure in the presence of internal cylinders with different R/bs at $Ra = 10^4$. As it can be seen in this figure, the Nusselt distribution has a maximum value at the point A which is the stagnation point on the top wall of the enclosure at the low R/bs. The thermal gradient increases at the point A. Because the isotherms take a distance from the upper surface of cylinder and they approach the top wall of enclosure. Therefore, at this point, the local Nusselt number has a greater value especially at low R/b ratios. Then the local Nusselt number decreases in the region A-C so that it takes a minimum value at the point C. When the R/b increases, the local Nusselt distribution from a certain value at the point A reaches a maximum value at the point B and then the Nusselt value decreases in the region B-C until it obtains its minimum value close to zero at the point C. Because the diameter of cylinder increases at large R/bs, the isotherms compress at the confined space between the cylinder and enclosure wall at the point B. Consequently, the Nussselt number takes a maximum value at this point. At the point C, due to reduction of flow intensity in the bottom half of enclosure and its increase in the upper half of enclosure, the thermal gradient decreases in the bottom part of enclosure. Consequently, the Nusselt value at this point will be lower than the Nusselt value at the point A.

The Fig. 8 shows the local Nusselt distribution along the wall of the elliptic enclosure at the different R/bs of inner cylinder and $Ra = 10^5$. As it can be observed in this figure, at the

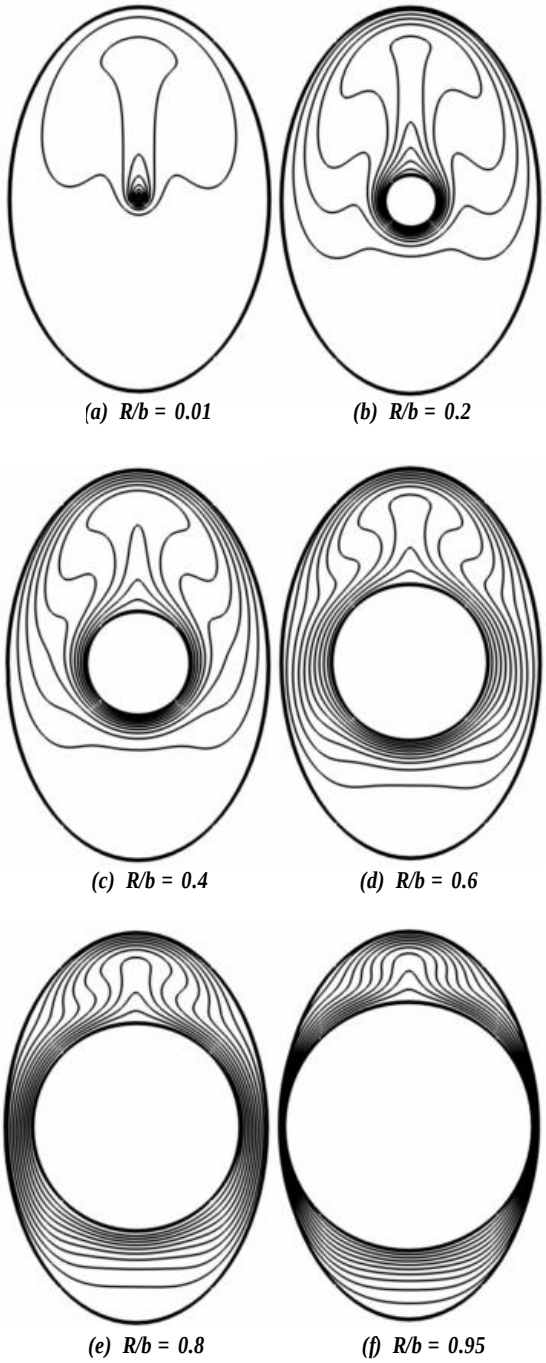

Fig. 5. The isotherms around the hot cylinder inside a cold elliptic enclosure at $Ra = 10^5$

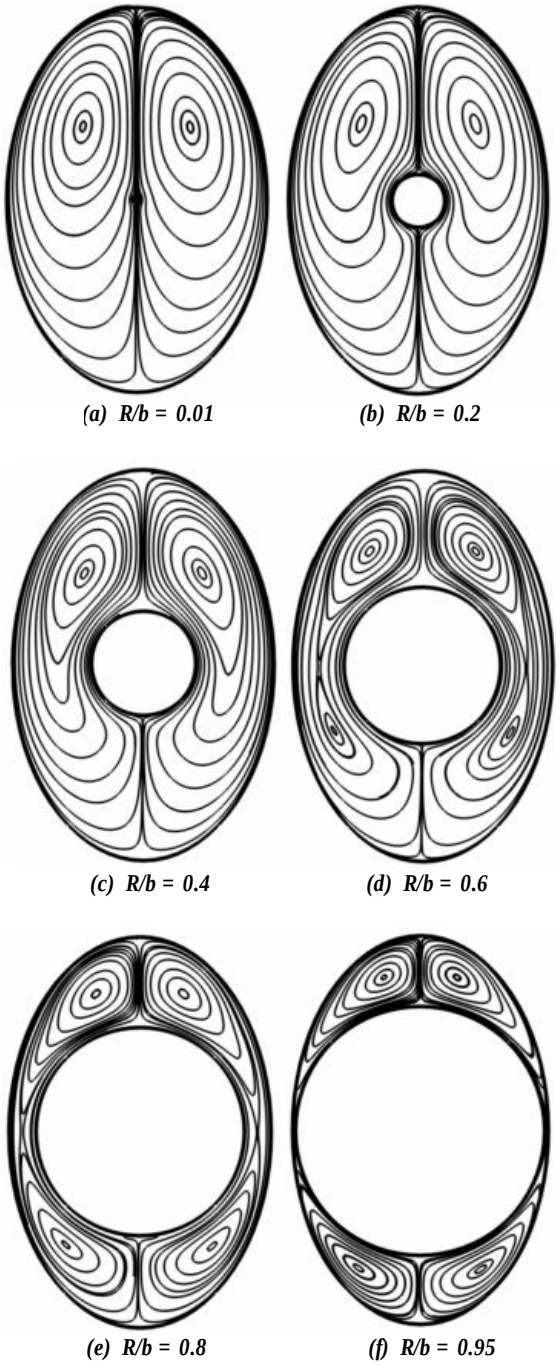

Fig. 6. The streamlines around the hot cylinder inside a cold elliptic enclosure at $Ra = 10^5$

first three ratios of R/b namely 0.01, 0.2 and 0.4, the local Nusselt distribution begin to decline from a maximum value at the point A until it reach a minimum value at the point C. In this case, increasing the Raleigh number, the natural convection becomes a predominant mechanism of heat transfer inside enclosure. Consequently, the flow intensity in upper half of enclosure increases than that in bottom half of enclosure. Subsequently, the isotherms move upward, causing a stronger thermal gradient in the upper part of the enclosure and a much lower thermal gradient in the lower part. Because of this, the Nusselt distribution begins with a maximum value at the point A and it reach a minimum value at the point C with a continuous negative slope. The Nusselt distribution is different in the other three ratios of R/b

in particular two ratios of 0.8 and 0.95. In these cases, first the Nusselt distribution starts from a local maximum value at the point A. Then with moving on the surface of enclosure and before reaching the point B, the Nusselt value decreases. This behavior can be justified according to the isotherm and streamline patterns at this Raleigh. Corresponding to the Fig. 5, the isotherms take a distance from the enclosure wall in the region B-C and their accumulation is reduced in this region. Because of this, the Nusselt distribution has a decline in this area. After the passage of this minimum value, the local Nusselt number starts to rise again so that it obtains a local maximum value at the point B. Then the Nusselt distribution starts to decline with uniform negative slope in the region B-C and it reach a minimum value at the point C. This is due to intensive effect of natural convection that causes to reduce flow intensity in bottom half of enclosure.

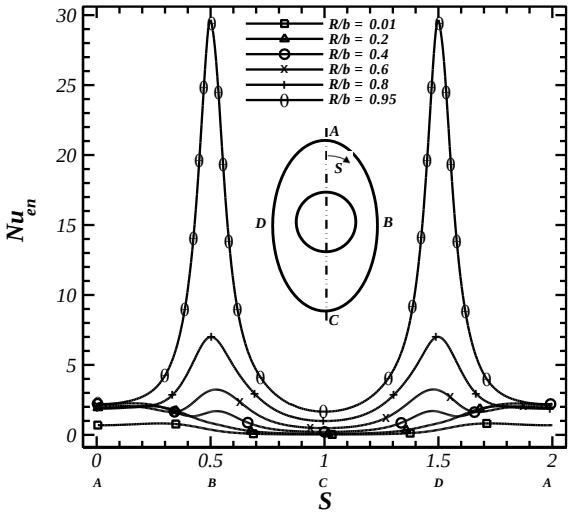

Fig. 7: Local Nusselt number distribution along the surface of the elliptic enclosure for different values of R/b at $Ra = 10^4$

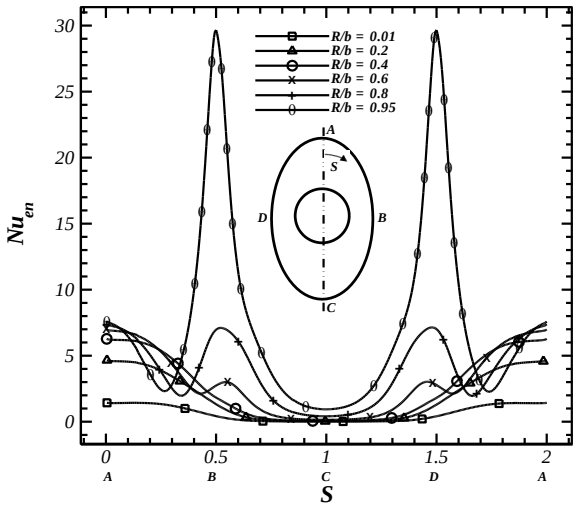

Fig.8: Local Nusselt number distribution along the surface of the elliptic enclosure for different values of R/b at $Ra = 10^5$

5.3. Average-Nusselt number of enclosure:

Fig. 9 presents the distribution of average-Nusselt number of elliptic enclosure in different values of R/b and studied Raleigh numbers. As it can be discerned in this figure with rising the R/b until 0.6, the Nusselt number go up almost linearly. After $R/b = 0.6$, the Nusselt increases exponentially. As an example of the results, when the R/b value changed from 0.2 to 0.6 at $Ra = 10^5$, the Nusselt number increased about 55 percent of its initial value. Moreover it is observed with increasing the Raleigh number, the Nusselt number is also increased so that when the Raleigh number is rose from 10^4 to 10^5 at $R/b = 0.6$, the Nusselt number climbed almost 65 percent of its initial value. As shown in this figure, increasing the Raleigh number, increase in the Nusselt value is different for each R/b. A obvious difference is observed in the Nusselt values with increasing the Raleigh number at low R/b ratios especially $R/b = 0.1$. This is because the inner cylinder diameter as a heat source and cause of fluid motion is small. Since the cylinder diameter is very small hence increasing the Raleigh number have not significant effect on the intensity of convective flow inside enclosure. But in medium ratios of R/b, increasing the Raleigh number, the difference between Nusselt values increases more. Especially this increase is obvious when the change is in high Raleigh numbers. This difference of Nusselt values decreases in large R/b ratios

similar to small R/b ratios. Because of increasing the diameter of cylinder with increasing the R/b ratios. Consequently, the space of fluid motion is dramatically reduced. Accordingly, the natural convection even in high Raleigh number is not considered as the only dominant mechanism of heat transfer and the conduction is considered as the significant mechanism of heat transfer too. Therefore at these R/bs, increasing the Raleigh number is not effective for enhancement of heat transfer rate.

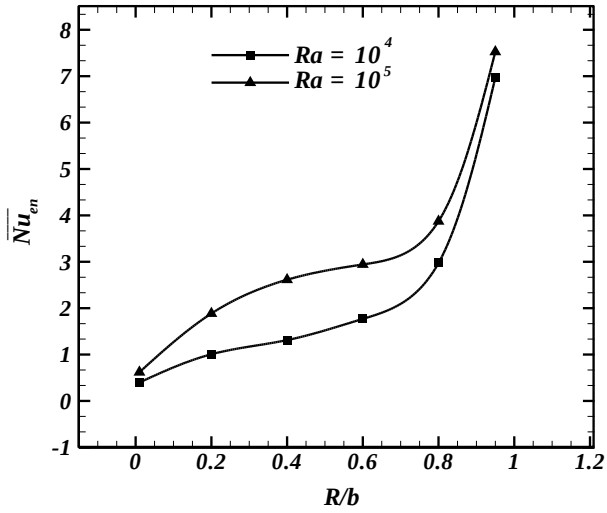

Fig. 9: Distribution of average-Nusselt number of elliptic enclosure in different values of *R/b* at four studied Rayleigh number

6. Conclusion

In the present paper, a two-dimensional simulation for parametric study of the effect of changing in R/b value on heat transfer rate from the cold elliptic enclosure has been performed. Governing equations have been solved using the finite volume method and TDMA in an ADI procedure for different values of R/b for the Rayleigh number 10^4 and 10^5. Results showed that The patterns of streamlines, isothermal lines and the Nusselt number values depended strongly on Rayleigh number and the R/b ratio. Moreover, it is observed with increasing Rayleigh number and R/b, heat transfer rate from the enclosure is increased. For example, by increasing Rayleigh number from 10^4 to 10^5, in the $R/b = 0.6$, average Nusselt enhanced about 65 percent of its initial value and by changing the R/b from 0.2 to 0.6, the average Nusselt climbed approximately 55 percent of its initial value at $Ra = 10^5$.

References

[1] X. Xu, Z.T. Yu, Y.C. Hu, L.W. Fan, K.F. Cen, Transient natural convective heat transfer of a low-Prandtl number fluid from a heated horizontal circular cylinder to its coaxial triangular enclosure, Int. J. Heat and Mass Transfer 55 (2012) 995-1003.

[2] M. Sheikholeslami, M. Gorji-Bandpy, D.D. Ganji, S. Soleimani, S.M. Seyyedi, Natural convection of nanofluids in an enclosure between a circular and a sinusoidal cylinder in the presence of magnetic field, Int. J. Heat and Mass Transfer 39 (2012) 1435–1443.

[3] R. Roslan, H. Saleh, I. Hashim, Effect of rotating cylinder on heat transfer in a square enclosure filled with nanofluids, Int. J. Heat and Mass Transfer 55 (2012) 7247-7256.

[4] A. da Silva, E. Fontana, V.C. Mariani, F. Marcondes, Numerical investigation of several physical and geometric parameters in the natural convection into trapezoidal cavities, Int. J. Heat and Mass Transfer 55 (2012) 6808-6818.

[5] A. Mark, E. Svenning, F. Edelvik, An immersed boundary method for simulation of flow with heat transfer, Int. J. Heat and Mass Transfer 56 (2013) 424-435.

[6] F. Oztop Hakan, M.M. Rahman, A. Ahsan, M. Hasanuzzaman, R. Saidur, Khaled. Al-Salem, N.A. Rahim, MHD natural convection in an enclosure from two semi-circular heaters on the bottom wall, Int. J. Heat and Mass Transfer 55 (2012) 1844-1854.

[7] M. Mahmoodi, S.M. Sebdani, Natural convection in a square cavity containing a nanofluid and an adiabatic square block at the center, J. Superlattices and Microstructures 52 (2012) 261-275.

[8] D. Mouhtadi, A. Amahmid, M. Hasnaoui, R. Bennacer, Natural convection in a horizontal channel provided with heat generating blocks: Discussion of the isothermal blocks validity, J. Energy Conversion and Management 53 (2012) 45-54.

[9] J.P.B. Mota, I.A.A.C. Esteves, C.A.M. Portugal, J.M.S.S. Esperanc, E. Saatdjian, Natural convection heat transfer in horizontal eccentric elliptic annuli containing saturated porous media, Int. J. Heat and Mass Transfer 43 (2000) 4367-4379.

[10] Y.D. Zhu, C. Shu , J. Qiu, J. Tani, Numerical simulation of natural convection between two elliptical cylinders using DQ method, Int. J. Heat and Mass Transfer 47 (2004) 797–808.

[11] S. J. Habeeb, Investigation of Heat Transfer Phenomena and Natural Flow Behavior around a Heated Square Cylinder Placed in a Cooled Elliptical Enclosure, Engineering and Technology journal 28 (2010) 702.

[12] H. Khozeymehnezhad, S.A. Mirbozorgi, Comparison of Natural Convection around a Circular Cylinder with a Square Cylinder Inside a Square Enclosure, J. Mechanical Engineering and Automation 2 (2012) 176-183.

[13] J. P. Van Doormaal, G. D. Raithby, Enhancement of the SIMPLE Method for Predicting Incompressible Fluid Flows, Numer. Heat Transfer 7 (1984) 147–163.

[14] C. M. Rhie, W. L. Chow, Numerical Study of the Turbulent Flow Past an Airfoil With Trailing Edge Separation, AIAA J. 21 (1983) 1525–1532.

[15] S. V. Patankar, Numerical Heat Transfer and Fluid Flow, McGraw-Hill, New York, 1980, pp. 52–54.

[16] B. Kim, D. Lee, M. Ha, H. Yoon, A numerical study of natural convection in a square enclosure with a circular cylinder at different vertical locations, Int. J. Heat and Mass Transfer 51 (2008) 1888-1906.